A quantum informed continuum model for ferroelectric materials

William Oates

Florida Center for Advanced Aero Propulsion (FCAAP), Florida A&M/Florida State University, Department of Mechanical Engineering, Tallahassee, FL 32310-6046, United States

E-mail: woates@fsu.edu

Abstract. *Quantum mechanical stress relations are studied to guide the development of a continuum scale electromechanical constitutive model for ferroelectric materials. Stresses at the quantum scale are determined through the use of the Hellmann-Feynman theorem to obtain an electrostatic stress that depends on the electric quadrupole density as opposed to polarization dependent electrostriction. The result is integrated into a continuum model using a generalized set of electronic coordinate vector order parameters contained within a Lagrangian density formulation. The new constitutive model is shown to be consistent with both the quantum based stress and classical phenomenological electrostriction. This conclusion is verified through a numerical study of lead titanate where calculations of energy, stress, and polarization from density functional theory (DFT) are fit to a continuum stored energy and electrostatic stresses. The numerical analysis includes uncertainty quantification using Bayesian statistics to gain further insight into material parameter uncertainty when approximating DFT calculations as a reduced-order continuum model.*

1. INTRODUCTION

Development of constitutive models that can predict macroscopic properties directly from the underlying changes of electron density still pose extraordinary computational challenges (Finnis 2012). Theoretical insights are desirable to introduce key material descriptions into reduced order models without complicating the equations with unnecessary parameters, higher order coupling, etc. Ferroelectric materials are an important class of smart materials that could benefit from such models that integrate key information at the quantum scale into a continuum model. These materials are well known for their extraordinary electromechanical characteristics used in a variety of adaptive structure applications, information storage, biomedical applications, and energy harvesting (Lines & Glass 1977, Jaffe et al. 1971, Eom & Trolier-McKinstry 2012, Smith 2005, Yang et al. 2010, Lynch 1996).

In support of this challenge, the Hellmann-Feynman theorem is utilized to guide the development of a reduced-order electromechanical continuum modeling framework. Quantum mechanical forces based on this theory are often used in DFT molecular dynamic calculations to determine relative positions of atomic nuclei as a function of the electrostatic forces between each atom (Gonze et al. 2009, Payne et al. 1992). The theorem quantifies forces between nuclei in solids based upon positive charges within the nuclei and interactions with the surrounding electrons (Feynman 1939). It is advantageous for continuum model development because it results in an electrostatic force instead of direct dependence on the quantum wave function (Weiner 1983, Feynman 1939). However, it still requires quantum calculations of the electron density. Despite this numerical challenge, practical aspects of this theorem are found to give a proportionality between stress and the electric quadrupole density which is conducive to continuum modeling approximations of ferroelectric materials and possibly other materials. Specifically, the underlying quantum relations provide input to a specific form of a continuum scale stored energy function such that the homogenized electromechanical stress also depends on a quadrupole density.

Macroscopic theories typically describe the electromechanical coupling in ferroelectric materials as electrostrictive, i.e., stress proportional to the square of the polarization (Lines & Glass 1977). Since the quadrupole density is the next higher order term in a Taylor series expansion of the electron density distribution, the energy due to dipoles is typically larger than energy associated with quadrupoles (Loudon 2000). However, Martin has argued that bulk piezoelectricity depends on both the polarization and the quadrupole density (Martin 1972). Similarly, ferroelectric nanostructures in the form of thin films, nanorods, and quantum dots have motivated further analysis of higher order electrical and mechanical effects (Catalan et al. 2011, Cross 2006, Lee et al. 2011). Questions about strain gradient induced polarization (i.e., flexoelectricity) has resulted in models that not only depend on the quadrupole density but also the octupole density (Resta 2010). This motivates the need for a stronger understanding of the correlation of local electronic structure with reduced order continuum models

capable of simulating the higher order electronic behavior in ferroelectric materials.

The continuum modeling framework starts with a Lagrangian density that contains free space energy of the electromagnetic fields, field-matter interactions, kinetic energy of the solid and stored energy of the solid (Nelson 1991, Nelson 1979). Acoustic and optical modes (i.e., electronic interactions) are treated using the center-of-mass point x_i and a set position vectors of charged particles within the lattice, y_i^ν with $\nu = 1, \ldots, n$, respectively. Both the center-of-mass and the charge particle position vectors are treated at the long-wavelength continuum limit. Homogenization over many unit cells within a ferroelectric domain is assumed in the continuum model such that an average position of the charge particles is taken as a smaller set of vector order parameters. In the analysis of lead titanate, the simplest case is assumed where the relative displacement of the lead, oxygen, and titanium atoms is modeled using a single vector order parameter. These electronic coordinates are used to quantify the polarization and the quadrupole density as

$$\begin{aligned} P_i &= J^{-1} \sum_\nu q^\nu y_i^\alpha \simeq \overline{q} y_i \\ Q_{ij} &= \frac{1}{2J} \sum_{\nu,\mu} q^{\nu\mu} y_i^\nu y_j^\mu \simeq \frac{1}{2} \overline{q} y_i y_j \end{aligned} \tag{1}$$

where $J = \det(F_{iK})$ is the determinant of the deformation gradient denoted by F_{iK} and y_i^ν is the position of a charged particle ν relative to the center-of-mass of the representative volume element. The effective charge densities representing each particle are denoted by q^ν and $q^{\nu\mu}$ for the polarization P_i and quadrupole density Q_{ij}, respectively. For lead titanate, the polarization and quadrupole density are approximated using a single vector order parameter y_i and effective charge density $\overline{q}$. In this approximation, small strain has been assumed where $J \simeq 1$. An illustration of the homogenized lead titanate unit cell is shown in Figure 1.

Electronic coordinate order parameters are introduced since they provide a means to quantify the polarization as well as higher order electric poles in a relatively compact set of governing equations. It is important to note however that a balance equation is required for each electronic coordinate within the homogenized unit cell. Thus, the approximation in the last relation on the right hand side in (1) is advantageous in reducing the set of coupled balance equations. But this raises questions on uncertainty associated with the evolution of charge density as a function of changes in stress or applied fields. This approximation becomes important in determining approximations of a continuum scale stored energy function. In this study, the stored energy and stress are calculated for different atomic displacements while holding the unit cell dimensions of the ferroelectric crystal fixed to a cubic reference state. In terms of continuum thermodynamics, this provides a means to fit a Landau- like energy function to DFT energy calculations at constant strain. Specifically, atoms within the unit cell are linearly incremented through the equilibrium tetragonal state that is determined from *ab initio* molecular dynamic DFT calculations.

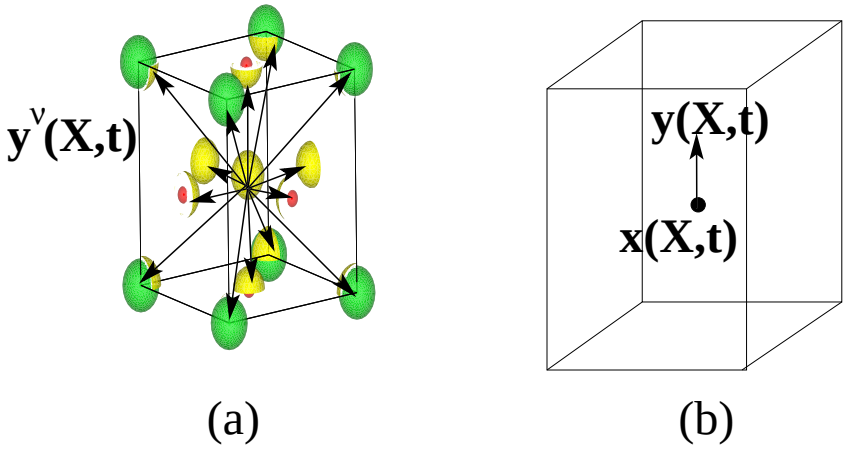

Figure 1. (a) Illustration of a high order model containing a large number of electronic coordinates ($\mathbf{y}^{\nu}(\mathbf{X},t)$ with $\nu = 1,\ldots,n$) describing charged particles within a ferroelectric unit cell. (b) Comparisons to the reduced order model containing only one electronic vector coordinate $\mathbf{y}(\mathbf{X},t)$ and its center-of-mass $\mathbf{x}(\mathbf{X},t)$.

The assumptions in going from a full DFT calculation of the electron density to a continuum description that uses one electronic coordinate order parameter clearly may lead to model parameter uncertainty. This issue is investigated by assuming the DFT calculations are exact while using Bayesian statistics to quantity uncertainty in the parameters and uncertainty propagation when calculating stress and energy at the continuum scale. Bayesian inference is different from the frequentist approach which quantifies model parameters as deterministic (Haario et al. 2001, Haario et al. 2006, Hu et al. 2012). The Bayesian method treats model parameters as random variables and quantifies the probability density functions (posterior densities) of the model parameters through comparisons to experimental data or higher fidelity models. The calculation of the posterior densities is an inverse problem requiring sampling over the space of possible parameter values. Often limited knowledge of the range of material parameter values is available excluding constraints from the first and second laws of thermodynamics. In this study, the error between the continuum model and DFT calculations is minimized by sampling over the expected range of possible continuum material parameter values using a Delayed Rejection Adaptive Metropolis (DRAM) algorithm (Haario et al. 2006). A likelihood function and a prior density are necessary to obtain the posterior density for each continuum model parameter. The prior density is the best estimate of the posterior density. In all simulations given here, a noninformative prior is used which is an un-normalized uniform density. The likelihood function converts information about sampling when computing the posterior density. It is classified as the conditional probability of the model given a set of model parameters.

In the following sections, the quantum mechanical stresses are first summarized followed by formulation of the electromechanical continuum model. This is followed

by the numerical analysis of lead titanate where the stored energy is quantified by incrementing internal atoms from the cubic state through the equilibrium tetragonal state. Energy, stress, and polarization based upon DFT computations are fit to the phenomenological continuum model. Markov chain Monte Carlo (MCMC) sampling and Bayesian statistics are used to quantify model uncertainty when homogenizing the DFT results as a continuum. Concluding remarks are given in the final section.

2. GOVERNING EQUATIONS

2.1. Quantum Mechanical Based Electrostatic Stress

The electrostatic potentials used to describe internal atomic interactions are given in terms of nuclei-nuclei, nuclei-electron, and electron-electron interactions

$$\begin{aligned} V_{nn} &= \frac{1}{4\pi\epsilon_0}\sum_{l,l'=1;l>l'}^{N}\frac{q_l q_{l'}}{s_{ll'}} = \frac{1}{4\pi\epsilon_0}\sum_{l,l'=1;l>l'}^{N}\frac{q_l q_{l'}}{\sqrt{\xi_{ll'}}} \\ V_{en} &= -\frac{1}{4\pi\epsilon_0}\sum_{l=1}^{N}\frac{eq_l}{s_{l\mathbf{r}}} = -\frac{1}{4\pi\epsilon_0}\sum_{l=1}^{N}\frac{eq_l}{\sqrt{\xi_{l\mathbf{r}}}} \\ V_{ee} &= \frac{1}{4\pi\epsilon_0}\sum_{i,j=1;i>j}^{M}\frac{e^2}{s_{ij}} = \frac{1}{4\pi\epsilon_0}\sum_{i,j=1;i>j}^{M}\frac{e^2}{\sqrt{\xi_{ij}}} \end{aligned} \tag{2}$$

where nuclei-nuclei relations are given in V_{nn}, nuclei-electron relations are given in V_{en}, and electron-electron interactions are given in V_{ee}. $\xi_{ll'} = s_{ll'}^2 = (\mathbf{x}_l - \mathbf{x}_{l'})^2$ is the squared distance between nuclei positioned at l and l', respectively, and $\xi_{l\mathbf{r}} = s_{l\mathbf{r}}^2 = (\mathbf{x}_l - \mathbf{r})^2$ is the squared distance between the nucleus at position l and the position of an electron at $\mathbf{r}$. The charges associated with these atomic nuclei are q_l and $q_{l'}$. Similarly, $\xi_{ij} = s_{ij}^2 = (\mathbf{r}_i - \mathbf{r}_j)^2$ describes the distances between electrons at the vector positions $\mathbf{r}_i$ and $\mathbf{r}_j$ for electrons i and j, respectively. The permittivity of free space is denoted by ϵ_0 and the magnitude of charge of an electron is denoted by e.

The forces between nuclei are used to define the stress in the solid. The Hellmann-Feynman theorem shows that the force on the nuclei can be described by the change in the potential with respect to the change in relative positions of the nuclei (Weiner 1983, Feynman 1939)

$$f_i = \frac{\partial V_{nn}}{\partial x_i(l)} + \int_\Omega \frac{\partial V_{en}}{\partial x_i(l)}\rho(\mathbf{r})dV. \tag{3}$$

The electron-electron interactions do not contribute to the force because the integration of the electron density is orthonormal and therefore leads to a potential gradient that is always zero. In this equation, the deformed position of each nuclei is given by $x_i(l)$. $\rho(\mathbf{r})$ is the electron density in the deformed crystal having volume Ω.

The forces on the nuclei can be reformulated into a measure of stress by first defining a deformation associated with the deformed nuclei positions relative to their reference positions. This is accomplished using the deformation gradient (Weiner 1983).

The discrete version of the deformation mapping material points from some reference position to a deformed position is

$$x_i(l) = F_{iK} X_K(l) \tag{4}$$

at each atomic nucleus cite l. The positions of the atoms at $t = 0$ are $X_K(l)$ and the deformation gradient is $F_{iK} = \dfrac{\partial x_i}{\partial X_K}$.

A few additional relations are introduced as follows to quantify the stress in terms of the second Piola-Kirchhoff stress. This requires defining the Lagrangian strain and how it influences changes in the atomic nuclei-nuclei and nuclei-electron potentials. First, the distance between atomic nuclei and electrons is defined in terms of the reference configuration as

$$\begin{aligned} \Delta X_K(ll') &= X_K(l) - X_K(l') \\ \Delta X_K(l\mathbf{R}) &= X_K(l) - X_K(\mathbf{R}) \end{aligned} \tag{5}$$

where $\Delta X_K(ll')$ describes the distance between atomic nucleus sites and $\Delta X_K(l\mathbf{R})$ describes the distance between an atomic nucleus site and an electron positioned at $\mathbf{R}$, all defined in the reference configuration. We then define the magnitude of squared length between atomic nucleus points and atomic nuclei-electron squared lengths to be

$$\begin{aligned} S^2_{ll'} &= \Delta X_K(ll')\Delta X_K(ll') \\ S^2_{l\mathbf{R}} &= \Delta X_K(l\mathbf{R})\Delta X_K(l\mathbf{R}). \end{aligned} \tag{6}$$

The Langrangian strain tensor, based on the atomic nuclei geometric changes, is then defined using continuum mechanics definitions (Malvern 1969, Weiner 1983)

$$\begin{aligned} s^2_{ll'} - S^2_{ll'} &= 2E_{KL}\Delta X_K(ll')\Delta X_L(ll') \\ s^2_{l\mathbf{R}} - S^2_{l\mathbf{R}} &= 2E_{KL}\Delta X_K(l\mathbf{R})\Delta X_L(l\mathbf{R}). \end{aligned} \tag{7}$$

We now substitute (7) into (3) to obtain the force in terms of the Lagrangian strain. This requires a relation between the potential gradient and changes in the potential with respect to strain. If we denote the total potential by $V_{tot} = V_{nn} + V_{en} + V_{ee}$, the change in the potential with respect to strain is

$$\frac{\partial V}{\partial E_{IJ}} = F^{-1}_{Ik} \sum_{l=1}^{N} \frac{\partial V}{\partial x_i(l)} X_J(l) \tag{8}$$

where F^{-1}_{Ik} is the inverse of the deformation gradient. The second Piola-Kirchhoff stress is then given by

$$\widetilde{T}_{IJ} = \frac{1}{\Omega_0}\left(\frac{\partial V_{nn}}{\partial E_{IJ}} + \int_{V_0} \frac{\partial V_{en}}{\partial E_{IJ}} \rho J^{-1} dV_0\right) \tag{9}$$

where Ω_0 is the volume of the material in the reference configuration.

Further manipulation of these geometric relations leads to

$$\widetilde{T}_{IJ} = \frac{1}{4\pi\epsilon_0\Omega_0}\left[-\sum_{l,l'=1;l>l'}^{N}\frac{q_l q_l'\Delta X_I(ll')\Delta X_J(ll')}{\sqrt{(2E_{KL}+\delta_{KL})^3[\Delta X_K(ll')\Delta X_L(ll')]^3}}\right.$$
$$\left.+\int\sum_{l=1}^{N}\frac{eq_l\Delta X_I(l\mathbf{R})\Delta X_J(l\mathbf{R})}{\sqrt{(2E_{KL}+\delta_{KL})^3[\Delta X_K(ll')\Delta X_L(ll')]^3}}\rho(\mathbf{r}(\mathbf{R}))J^{-1}dV_0\right] \tag{10}$$

and in the small strain limit where all components of $E_{IJ} << 1$, we have

$$\widetilde{T}_{IJ} = \frac{1}{4\pi\epsilon_0\Omega_0}\left[-\sum_{l,l'=1;l>l'}^{N}\frac{q_l q_l'\Delta X_I(ll')\Delta X_J(ll')}{\sqrt{(\Delta X_K(ll')\Delta X_K(ll'))^3}}\right.$$
$$\left.+\int\sum_{l=1}^{N}\frac{eq_l\Delta X_I(l\mathbf{R})\Delta X_J(l\mathbf{R})}{\sqrt{(\Delta X_K(ll')\Delta X_K(ll'))^3}}\rho(\mathbf{r}(\mathbf{R}))J^{-1}dV_0\right] \tag{11}$$

where the nuclei-dependent stress in the first term is a constant since $\Delta X_I(ll')$ is fixed to the reference configuration. The second term contains the electron density which may change during deformation or applied fields. Any asymmetry in the electron density may lead to anisotropic stress and deformation often observed in ferroelectric materials. Importantly, this second stress component is proportional to the quadrupole which is defined by (Panofsky & Phillips 1962)

$$Q_{IJ} = \int\rho(\mathbf{r}(\mathbf{R}))\Delta X_I(l\mathbf{R})\Delta X_J(l\mathbf{R})J^{-1}dV_0. \tag{12}$$

A direct calculation of this stress is not trivial due to the difficulty in obtaining the electron density and correlating it with the integral in (11). This stress will be approximated using DFT simulations to estimate the electron density. Prior to calculation of the DFT stresses, we introduce continuum based stresses from a homogenized stored energy function and illustrate what is required to obtain an electrostatic stress that is proportional to a quadrupole density.

2.2. Nonlinear Continuum Model

The continuum formulation makes use of a Lagrangian density summarized in (Nelson 1979, Nelson 1991). Key equations are summarized here to motivate the comparisons to the quantum relations. The model includes energy in free space, electromagnetic interactions with matter, and material energy that initially includes both kinetic and stored energy. The kinetic energy is decomposed into acoustic and optical mode behavior. This form facilitates modeling electronic behavior in terms of a set of electronic vector order parameters that can describe polarization, quadrupole densities, and higher order poles.

In the spatial frame, the Lagrangian density is concisely described for the free space and interaction terms as

$$\mathcal{L}_{FS} = \frac{\epsilon_0}{2}E_iE_i - \frac{1}{2\mu_0}B_iB_i$$
$$\mathcal{L}_{IS} = J_iA_i - q\Phi \tag{13}$$

where in the free space Lagrangian energy density, $\mathcal{L}_{FS}$, is a function of the electric field E_i, magnetic flux density B_i, permittivity of free space ϵ_0, and permeability of free space μ_0. The interaction Lagrangian density, $\mathcal{L}_{IS}$, is a function of the current density J_i, magnetic vector potential A_i, bound charge density q, and electrostatic potential Φ. Both energy densities are written per deformed volume and the fields are written in the spatial frame.

The material's kinetic and stored energy densities are more easily written per undeformed volume as

$$\mathcal{L}_{MM} = \frac{\rho^0}{2}\dot{x}_i\dot{x}_i + \sum_\nu \frac{m^\nu}{2}\dot{y}_i^\nu\dot{y}_i^\nu - \rho^0\Sigma(E_{IJ}, \Pi_I^\nu) \tag{14}$$

where the first term on the right hand side is kinetic energy in terms of the center-of-mass point velocity field $\dot{x}_i$ and density per reference volume ρ^0. The second term is the set of electronic interactions that give rise to optical modes where $\dot{y}_i^\nu$ is the velocity of the charge particles and m^ν is the mass density per reference volume for the respective charged particles. The last term is the stored energy written as a function of the Lagrangian strain E_{IJ} and the rotational invariant form of the electronic coordinate position Π_I^ν.

Rotational invariance on the electronic order parameters is satisfied using

$$\Pi_I^\nu = F_{Ik}^{-1} y_k^\nu \tag{15}$$

where F_{Ik}^{-1} is the inverse deformation gradient (Nelson 1979).

Through minimization of these three Lagrangian densities, a set of governing equations are obtained which include linear momentum, two of the four time dependent Maxwell's equations, and an electronic force balance equation. The other two of Maxwell's equations are obtained through identities between the electrostatic potential, magnetic vector potential, and field relations (Loudon 2000). For completeness, these equations are summarized below starting with Maxwell's equations

$$\begin{aligned} e_{ijk}E_{k,j} &= -\frac{\partial B_i}{\partial t} \\ e_{ijk}B_{k,j} &= \mu_0\left(\epsilon_0\frac{\partial E_i}{\partial t} + J_i\right) \\ \epsilon_0 E_{i,i} &= q \\ B_{i,i} &= 0 \end{aligned} \tag{16}$$

subject to the boundary conditions

$$\begin{aligned} K_k &= H_i e_{kij} n_j \\ \omega_D &= -D_i n_i \\ e_{kij}E_i n_j &= 0 \\ B_i n_i &= 0 \end{aligned} \tag{17}$$

where K_k is the surface current, ω_D is the surface charge, and the remaining two equations require tangential electric fields to be continuous and normal magnetic flux density components to be continuous across a surface. This surface is denoted by its outward pointing unit normal components n_i.

Linear momentum based on this Lagrangian density is

$$\rho\frac{d^2x_i}{dt^2} = \sigma^E_{ji,j} + qE_i + e_{ijk}J_jB_k \tag{18}$$

subject to either traction or constrained displacements on the surface.

Lastly, the electronic balance equation is

$$m^\nu\ddot{y}^\nu_i + \frac{\partial\rho^0\Sigma}{\partial y^\nu_i} = q^\nu E_i + \sum_\nu q^{\nu\mu}y^\mu_j E_{i,j} + e_{ijk}\dot{x}_j\sum_\mu q^{\nu\mu}y^\mu_l B_{k,l}. \tag{19}$$

This equation contains individual charge densities associated with each vector order parameter as denoted by q^ν and $q^{\nu\mu}$. They are related to the definition of polarization and quadrupole densities given previously in (1). The coupling between these electric moments and the Langrangian densities occurs through the interaction Lagrangian density based on the definition of the current density and charge density

$$\begin{aligned} J_i(\mathbf{z},t) &= \frac{\partial P_i}{\partial t} + (P_i\dot{x}_j)_{,j} - (P_j\dot{x}_i)_{,i} - \frac{\partial Q_{ji,j}}{\partial t} - (Q_{ij}\dot{x}_k)_{,jk} + (Q_{jk}\dot{x}_i)_{,jk} \\ q &= -P_{i,i} + Q_{ij,ij} \end{aligned} \tag{20}$$

where we have neglected magnetization effects.

Particular interests is placed on the form of the Cauchy stress σ^E_{ij}. It can be shown that a compact form of this stress is

$$\sigma^E_{ij} = J^{-1}F_{jK}F_{iL}\frac{\partial\rho^0\Sigma}{\partial E_{KL}} + \sum_\nu \rho^\nu\ddot{y}^\nu_i y^\nu_j - (Q_{jl}E_i)_{,l} \tag{21}$$

where the first stress component is the conventional "mechanical" stress written as a function of changes in stored energy with respect to changes in the Lagrangian strain. The second term is an optical effect which can become important when the material strongly absorbs electromagnetic radiation. This term has used the notation on the mass density per deformed volume, $\rho^\nu = J^{-1}m^\nu$. The last term is a function of the gradient of the product between the quadrupole density and the electric field. Note that this Cauchy stress does not include Maxwell stresses in free space. These stresses must be added to (21) to obtain the total Cauchy stress (Nelson 1979). In all subsequent analysis, we focus on electrostatic stresses in a single ferroelectric domain such that the second and third terms in the stress equation are zero. The applied field will also be zero such that stresses in a vacuum are zero.

2.3. Continuum Scale Stored Energy

A stored energy function is written in terms of the Lagrangian strain and a single electronic vector order parameter to quantify quasi-static stresses in a single ferroelectric domain. This vector order parameter represents a normalized atomic displacement between the lead, titanium, and oxygen atoms. In the continuum scale stored energy function given as follows, the superscript on Π_I^ν is omitted. Section 3 goes into more detail about how the single vector order parameter describes the atomic behavior within a unit cell of lead titanate.

The stored energy is proposed to be

$$\begin{aligned}\rho^0\Sigma = \frac{c_{IJKL}}{2}E_{IJ}E_{KL} - b_{IJKL}E_{KL}\Pi_I\Pi_J + \frac{A}{2}\Pi_I\Pi_I + \\ + \frac{B\delta_{IJKL}}{4}\Pi_I\Pi_J\Pi_K\Pi_L + \frac{C}{4}\Pi_I\Pi_J\Pi_I\Pi_J\end{aligned} \tag{22}$$

where c_{IJKL} is the elastic tensor, b_{IJKL} is the field-coupled tensor, and the Landau parameters are A, B, and C. A Kronecker delta δ_{IJKL} has been introduced which is equal to one if $I = J = K = L$ and otherwise zero. Using this form, the "mechanical" Cauchy stress is defined by $\sigma^y_{ij} = J^{-1}F_{jK}F_{iL}\dfrac{\partial\rho^0\Sigma}{\partial E_{KL}}$ which gives

$$\sigma^y_{ij} = J^{-1}F_{iK}F_{jL}\left(c_{IJKL}E_{IJ} - b_{IJKL}\Pi_I\Pi_J\right) \tag{23}$$

Lead titanate exhibits small strain such that the mechanical Cauchy stress can be approximated in the small strain limit ($E_{IJ} \to \epsilon_{ij} = 1/2(u_{i,j} + u_{j,i})$ where u_i is displacement). In this case, (23) simplifies to

$$\sigma^y_{ij} = c_{ijkl}\epsilon_{kl} - b_{ijkl}\Pi_k\Pi_l \tag{24}$$

where the small strain assumption requires the deformation gradient to be approximately the identity matrix and $J \simeq 1$ which leads to $\Pi_i \simeq y_i$. The upper and lower case indices within the tensors also become equivalent in the small strain limit.

It is important to note that the second stress component in this equation contains a quadratic dependence on the electronic vector order parameter or equivalently, linear coupling to the quadrupole density. The coupling in the stored energy was chosen in this form to be analogous to the Hellmann-Feynman quadrupole stress given in Section 2.1. It is also analogous to classical electrostriction used to describe many ferroelectric materials. In the following section, we quantify the material parameters in this stored energy function by comparing them to energy and stress obtained from DFT calculations.

3. NUMERICAL ANALYSIS

The numerical analysis includes DFT calculations for lead titanate followed by comparisons to the continuum model using Bayesian statistics. Model parameters for the continuum model are obtained by minimizing the sum of the squares of the error between the continuum energy and stress versus the DFT energy and stress.

3.1. Lead Titanate DFT Calculations

First the low energy, zero stress state is calculated as a function of the electron density by optimizing both the ionic positions within the unit cell and the unit cell lattice dimensions. The minimization method is based on the Broyden-Fletcher-Goldfard-Shanno method contained within Abinit 7.0.5 (Gonze et al. 2009). Previously developed pseudopotentials contained within this code were used to approximate the higher order behavior of the wave function near atomic nuclei. All DFT simulations were run using a $10 \times 10 \times 10$ k-point grid on a five atom unit cell with a cut-off energy of 60 Ha (1633 eV). The local density approximation was used in all calculations.

The equilibrium tetragonal lattice parameters and relative atomic positions within the lattice are given in Table 1 illustrating reasonable estimates relative to experimental measurements (Shirane et al. 1956, Mabud & Glazer 1979). The notation for the oxygen molecules follows the notation in (Shirane et al. 1956). The oxygen $O_I(+/-)$ are on the top and bottom unit cell faces, respectively. The label O_{II} refers to the other four oxygen on the remaining four sides of the unit cell. The corresponding electron density in the fully relaxed tetragonal state is plotted in Figure 2. This lowest energy tetragonal crystal atomic configuration is used as a reference for comparisons to internal atomic changes towards a cubic state and towards a state of larger tetragonality.

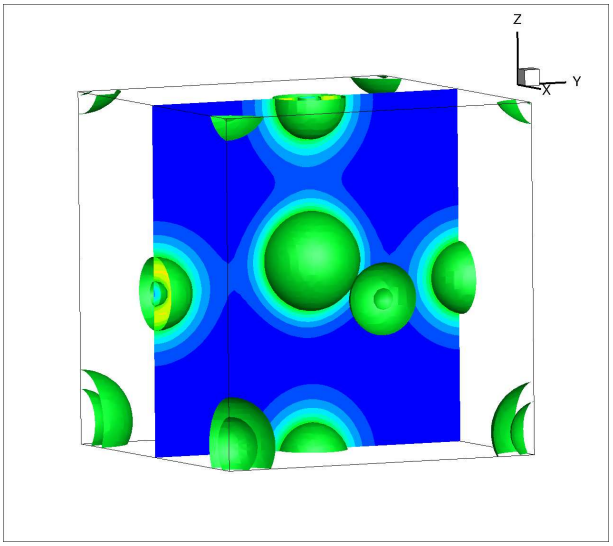

Figure 2. Plot of the electron density within a unit cell of lead titanate at the lowest energy tetragonal state. Titanium is the center atom and lead is on each corner. The labels for oxygen in Table 1 include $O_{I(+)}$ on the top, $O_{I(-)}$ on the bottom, and O_{II} on the four sides.

Since the independent variables in the continuum stored energy are E_{IJ} and Π_I, the unit cell dimensions are held fixed and the internal atomic positions are incremented to quantify changes in stored energy with respect to Π_I. We arbitrarily use a reference cubic lattice cell when incrementing Π_I. The unit cell lattice dimensions were compressed into a cubic state such that its lattice dimensions were $a \times a \times a$. Given this unit cell size, the relative positions of the oxygen, titanium, and lead atoms were linearly incremented relative to their equilibrium tetragonal state positions. Note however that the atomic

positions were incremented relative to the $a \times a \times a$ size unit cell and not the $a \times a \times c$ unit cell. The energy, stress, and polarization were computed for each incremental change in the atomic configurations. The polarization due to these internal atomic position changes was determined using the Berry phase approach within Abinit (Gonze et al. 2009, Resta & Vanderbilt 2007).

The degree of tetragonality, as a function of the internal atomic positions, is defined for spontaneous polarization aligned in the X_3 direction. In this case, the changes in each atom within the unit cell are described by

$$\begin{aligned} \Pi_3^{O_\perp} &= \alpha \Pi_3 \\ \Pi_3^{Pb} &= \beta \Pi_3 \\ \Pi_3^{O_\parallel} &= \gamma \Pi_3 + \mu \\ \Pi_3^{Ti} &= \nu \Pi_3 + \mu \end{aligned} \tag{25}$$

where $\alpha, \beta, \gamma, \mu$ and ν are constants given in Table 2. These constants are determined based on the calculated equilibrium lattice configuration summarized in Table 1. Π_3 has been normalized with respect to the equilibrium tetragonal state. For example, a value of $\Pi_3 = 1$ describes the equilibrium tetragonal state while $\Pi_3 = 0$ describes the cubic state. The change in polarization is plotted as a function of the increments of Π_3. An approximately linear relation between Π_3 and P_3 is illustrated in Figure 3. Note that the polarization at the equilibrium tetragonal state was calculated to be 0.81 C/m^2 using the Berry phase approach. Experimental values of polarization in lead titanate can vary significantly from 0.5 to 1.0 C/m^2 (Lines & Glass 1977). Comparisons of the present calculation with other DFT psuedopotentials (Bilc et al. 2008) illustrate the spontaneous polarization may range between 0.78 to 1.4 C/m^2. A value of 0.78 C/m^2 was predicted using LDA by Bilc et al. thus illustrating reasonable self-consistency with

Table 1. A summary of the lattice constant calculations using the local density approximation (LDA) within Abinit and comparisons to experimental results (Shirane et al. 1956, Mabud & Glazer 1979). The lattice parameter a and bond distances between atomic nuclei are in Angstroms.

	LDA	Experimental
a	3.858	3.904
c/a	1.045	1.064
$Ti - O_{I(-)}$	2.24	2.38
$Ti - O_{I(+)}$	1.90	1.78
$Ti - O_{II}$	1.95	1.98
$Pb - O_I$	2.75	2.80
$Pb - O_{II(+)}$	2.50	2.53
$Pb - O_{II(-)}$	2.73	3.20

the present analysis.

Table 2. The parameters below have all been normalized with respect to the cubic lattice parameter $a = 3.858$ $\mathring{A}$. The dimensional parameters are scaled to obtain the values in (25), (e.g., $\alpha = \overline{\alpha}a$, $\beta = \overline{\beta}a$, etc.).

$\overline{\alpha}$	$\overline{\beta}$	$\overline{\gamma}$	$\overline{\mu}$	$\overline{\nu}$
-0.02838	0.0639	0.4577	0.5000	0.5281

Shearing the internal atomic configuration is also required to quantify all parameters in the stored energy as a function of Π_I. This is non-trivial using DFT calculations since periodic lattice cells are implemented in the computations. Displacement of the oxygen O_{II} and titanium with respect to the lead and oxygen O_I leads to oscillatory shearing on the order of the unit cell dimensions. Supercell DFT computations that contain a region of free space are expected to provide information about shear electromechanics, but are not considered here.

Based on tetragonal symmetry, the stored energy density from (22) is simplified in

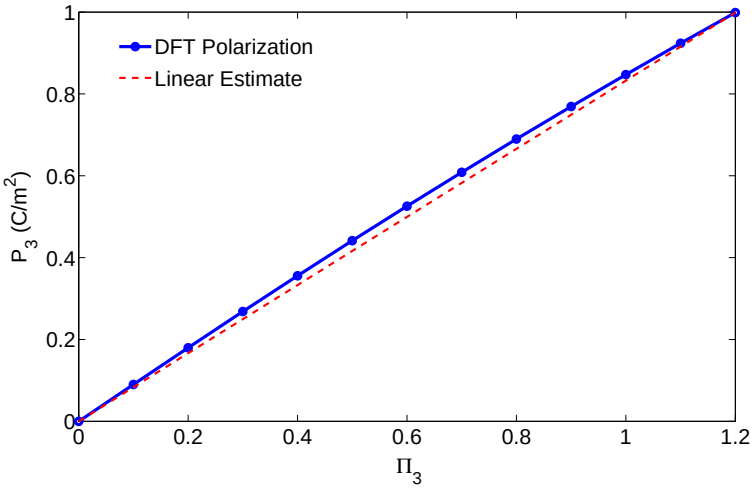

Figure 3. Polarization calculations from DFT calculations with respect to the normalized variable Π_3 from (25). The polarization was determined using the Berry phase approach (Resta & Vanderbilt 2007). A comparison to linearity is shown in (a) by plotting the polarization against the straight dotted line.

terms of a reduced set of materials coefficients

$$\begin{aligned}\rho^0\Sigma = \frac{c_{ijkl}}{2}\epsilon_{ij}\epsilon_{kl} - b_1\left(\epsilon_{11}\Pi_1^2 + \epsilon_{22}\Pi_2^2 + \epsilon_{33}\Pi_3^2\right) - b_2\Big(\varepsilon_{11}(\Pi_2^2+\Pi_3^2)\\ +\epsilon_{22}(\Pi_1^2+\Pi_3^2) + \epsilon_{33}(\Pi_1^2+\Pi_2^2)\Big) - b_3\left(\epsilon_{12}\Pi_1\Pi_2 + \epsilon_{13}\Pi_1\Pi_3 + \right.\\ \left.\epsilon_{23}\Pi_2\Pi_3\right) + \frac{A}{2}\left(\Pi_1^2+\Pi_2^2+\Pi_3^2\right) + \frac{B}{4}\left(\Pi_1^4+\Pi_2^4+\Pi_3^4\right) + \\ \frac{C}{2}\left(\Pi_1^2\Pi_2^2 + \Pi_1^2\Pi_3^2 + \Pi_2^2\Pi_3^2\right).\end{aligned} \tag{26}$$

where we have assumed small strain by implementing ϵ_{ij}. The parameters A, B, b_1, and b_2 are quantified numerically since shear effects associated with C and b_3 are not considered. The atomic increments are all made on a fixed unit cell with lattice dimensions $a \times a \times a$ which results in an unknown residual stress that is determined by comparing continuum stresses to the DFT stresses by subtracting $\sigma_{ij}^R = \sigma^R\delta_{ij}$ from the right hand side of (24).

Components of the Cauchy stress are obtained from the derivative of the stored energy plus the residual stress as

$$\begin{aligned}\sigma_{11}^y &= c_{11}\epsilon_{11} + c_{12}\epsilon_{22} + c_{13}\epsilon_{33} - b_2\Pi_1\Pi_1 - b_1\left(\Pi_2\Pi_2 + \Pi_3\Pi_3\right) + \sigma^R\\ \sigma_{33}^y &= c_{13}\epsilon_{11} + c_{13}\epsilon_{22} + c_{33}\epsilon_{33} - b_2\Pi_3\Pi_3 - b_1\left(\Pi_1\Pi_1 + \Pi_2\Pi_2\right) + \sigma^R\end{aligned} \tag{27}$$

where we have implemented Voigt notation on the elastic constants (Malvern 1969). Since the unit cell dimensions are held fixed, all strain components are zero. Focused is therefore placed on identifying the uncertainty in the electromechanical coefficients b_1 and b_2.

In the following section, it is shown that reasonable fits to the stored energy and stress are obtained over relative large changes in Π_3. Bayesian statistics illustrate relatively low uncertainty in all four parameters A, B, b_1 and b_2. Simulations were initially run by minimizing error between both the energy and stress. It was confirmed that no correlation occurs among the Landau parameters and the electromechanical parameters. This is because the strain is held fixed in all simulations. Subsequent simulations were conducted by sampling the parameter space and minimizing the error between the energy and stress separately. The Bayesian statistics were found to be practically identical in the two cases.

3.2. Continuum Model Uncertainty Quantification

Bayesian statistics are used to quantify material parameter uncertainty associated with fitting the phenomenological constants in (26) and (27) to DFT calculations. The sum of least squares of the error is minimized between the DFT and continuum energy and stress calculations. Markov chain Monte Carlo (MCMC) simulations using the DRAM algorithm (Haario et al. 2006) were run for 2×10^5 iterations to obtain statistical information about each continuum model parameter. Larger simulations were also run with 1×10^6 iterations; however, differences in the statistical results were negligible.

Table 3. A summary of the phenomenological parameters fit to the DFT energy in Figure 4. All units are in GPa. Parameters were determined using 2×10^5 iterations.

Parameter	Mean	Standard Deviation
A	-0.510	0.023
B	1.54	0.039
b_1	2.27	0.143
b_2	13.10	0.142
σ^R	-3.94	0.081

The errors were initially computed by simultaneously quantifying and minimizing errors between the energy and stress. However, since all the simulations were run at a fixed unit cell and thus zero strain, the energy and stress were decoupled. This allowed for separate MCMC optimization calculations to be run on the energy and stress. The minimization for these two cases are

$$\begin{aligned} SS_E &= \sum_i (E^{DFT}[i] - \Sigma[i])^2 \\ SS_\sigma &= \sum_i \left[(\sigma_{11}^{DFT}[i] - \sigma_{11}^{y}[i])^2 + (\sigma_{33}^{DFT}[i] - \sigma_{33}^{y}[i])^2 \right] \end{aligned} \tag{28}$$

where E^{DFT} denotes the DFT energy and similarly, the DFT superscript corresponds to stress calculations from DFT simulations. The notation $[i]$ corresponds to each atomic configuration simulated ranging from the cubic to the tetragonal state.

Table 3 illustrates the mean and standard deviation of the phenomenological parameters determined from fits to the DFT model. Using the mean values, the fits for energy and stress are illustrated in Figure 4 which show good estimates using a single order parameter Π_i over the range of atomic structure and electronic changes. The total energy from the DFT calculations were normalized with respect to the cubic unit cell volume, $V_0 = 61.46$ $\mathring{A}^3$. It is important to note that the energy minimum is not located at the spontaneous polarization calculation of 0.81 C/m^2. All energy calculations were conducted over a fixed unit cell of $a \times a \times a$ instead of the relaxed $a \times a \times c$ unit cell where spontaneous polarization was calculated after minimizing the energy as a function of both the atomic position and unit cell. The minimum energy polarization in the constrained cubic state is reduced to approximately 0.53 C/m^2. This reduction in polarization is expected since the unit cell has been compressed. It is also worth noting that changes in electromechanical normal stresses are approximately linear with respect to $\Pi_i \Pi_j$ as shown in Figure 4(b). This is qualitatively equivalent to the quantum based quadrupole stress given by the second term in (11). The result is also self-consistent with conventional electrostrictive models that assume stress is proportional to the polarization squared (Lines & Glass 1977).

Statistical information about the stored energy parameters A and B, electromechanical coupling coefficients b_1 and b_2, and residual stress σ^R are quantified using Bayesian

statistics. The DRAM algorithm was implemented to sample material parameters over the expected range of possible values. Large bounds were implemented to ensure a sufficiently broad range of values were considered when minimizing errors. The sampling space of all five parameters over 2×10^5 iterations is plotted in Figure 5 highlighting the values have reached 'burn-in' since there is no large shift in the mean over the set of iterations. This is facilitated by the initial guess and implementing a MCMC pre-run of 1000 iterations. The output of the smaller pre-run are input to the larger simulation containing 2×10^5 iterations.

The nominal values from Figure 5 can be compared to the summary of the mean values and standard deviations previously given in Table 3. Additional statistical information is provided by plotting the posterior probability densities shown in Figure 6 which illustrate all parameters form a symmetric density that is approximately Gaussian.

A correlation of all five material parameters is plotted in Figure 7 to determine if there are any dependencies among the parameters. These simulations were conducted initially by combining the two sums of error equations in (28). There is strong correlation among the two Landau parameters and weaker correlation among the electromechanical coupling and residual stress. Decoupling between the Landau and stress parameters is expected since all simulations were run for the case of zero strain. The inverse linear correlation between A and B is expected over the range of Π_3 considered since these two values are competing against one another to shift the minimum to different values of Π_3.

Based on the Bayesian statistical calculations illustrated in Figures 5 and 6, the propagation of uncertainties in the continuum energy and electrostatic stresses is plotted in Figure 8. The uncertainty propagation uses the chains from Figure 5 and plots both

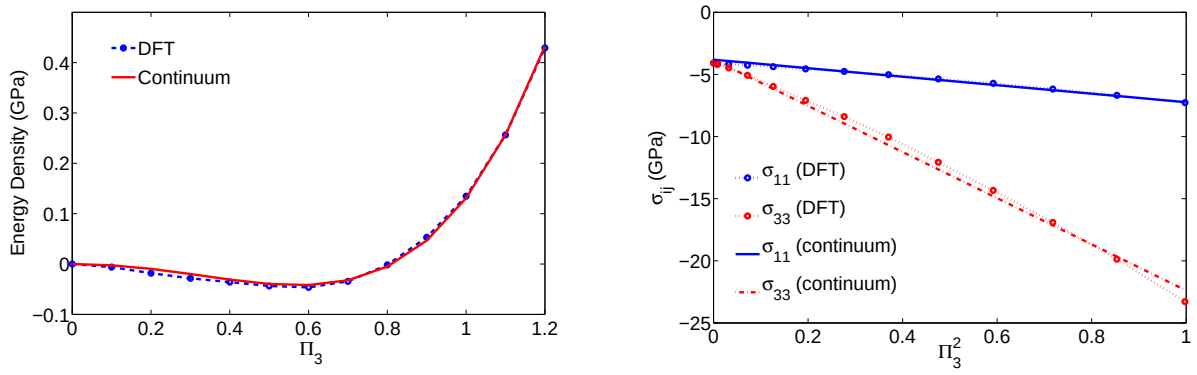

(a) (b)

Figure 4. (a) DFT energy calculations and comparisons to a model fit given by (26). The energy is plotted as a function of the electronic coordinate vector component Π_3. (b) Error propagation of the energy due to parameter uncertainty of A and B.

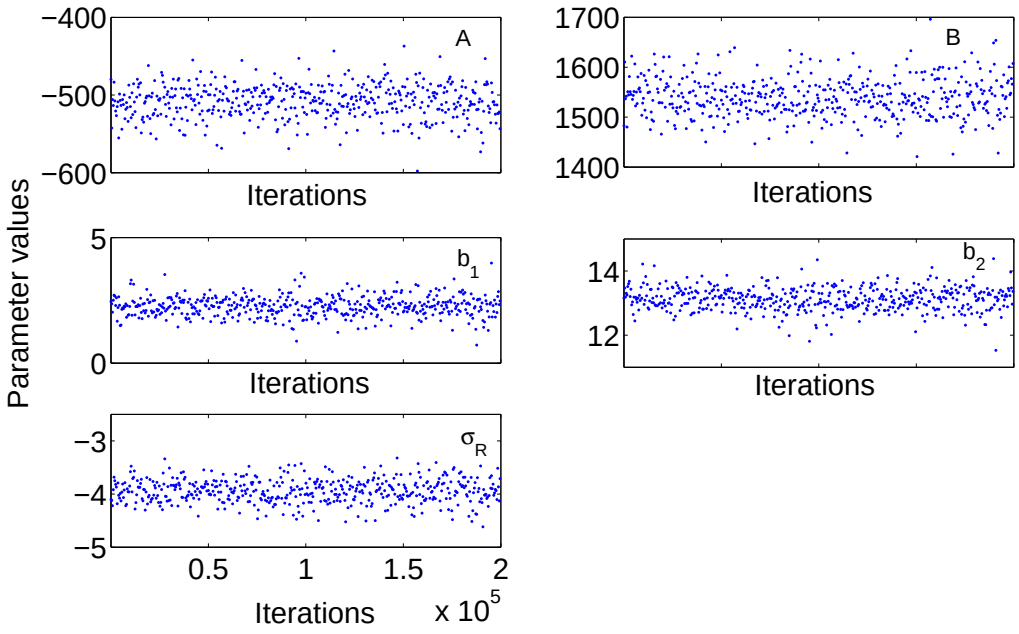

Figure 5. Illustration of the MCMC model parameter sampling over a set of 2×10^5 iterations for each parameter.

the 99% and 95% confidence intervals relative to the mean continuum estimates and DFT results. As previously given in Table 3, the standard deviations of all five parameters is small relative to their mean values. This was confirmed by calculating the uncertainty propagation as illustrated in the 99% confidence intervals for the energy and electrostatic stresses as shown in Figure 8.

4. CONCLUDING REMARKS

Quantum mechanical stresses based upon the Hellmann-Feynman theorem were used to guide the formulation of a continuum approximation of electrostatic stresses in ferroelectric materials. The theoretical results illustrate how electrostatic stresses based upon atomic potentials of interacting charged nuclei and surrounding electrons result in a stress component that is proportional to the electric quadrupole density. This result was used to guide the formulation of a relatively general continuum model that describes electrostatic stresses in solids. The continuum model, based upon prior studies from (Nelson 1991, Nelson 1979), was extended by formulating a stored energy function that contained particular quadrupole density coupling in terms of electronic vector order parameter coupling with strain. These results provide consistency between quadrupole stresses from the Hellmann-Feynman theorem as well as phenomenological

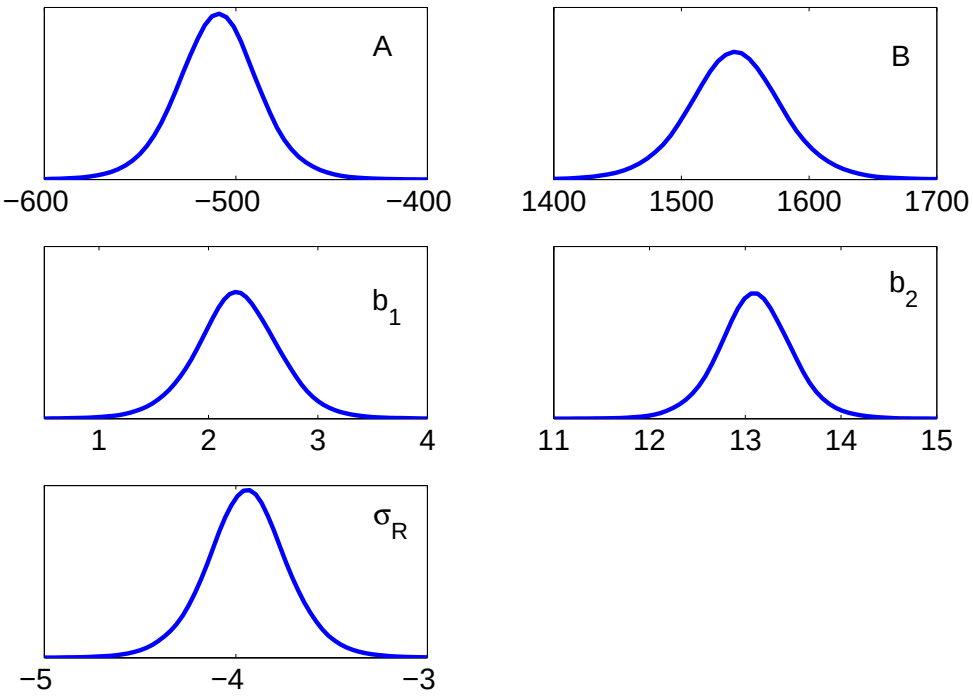

Figure 6. Bayesian calculations of the probability densities for the continuum model parameters and residual stress. The y-axis represents the probability value as a function of the possible values of each parameter along the x-axis.

electrostrictive stresses that depend quadratically on the polarization.

The general form of the continuum model contained electronic coordinate vector order parameters Π_I^ν with $\nu = 1, \ldots, n$ representing the position of charged particles within a representative volume element. The simplified model for tetragonal phase ferroelectric materials assumed a model reduction to a single vector order parameter. Whereas this resulted in a model equivalent to conventional electrostriction, the results are relatively general and may potentially be extended to more complex electronic structure evolution in ferroelectric solids. This reduced order assumption is anticipated to become important under complex, multi-axial loading or near defects in ferroelectric materials.

The model was numerically validated by comparing DFT computations of lead titanate to the homogenized continuum model. Changes in the internal electronic state were computed using DFT by incrementing atom positions about fixed increments from a cubic state through the equilibrium tetragonal state. This resulted in a set of energy, stress, and polarization calculations that were defined as the 'true' material state. However, the computations only considered a range of Π_I values parallel to the spontaneous polarization of lead titanate which is limited to one dimensional behavior.

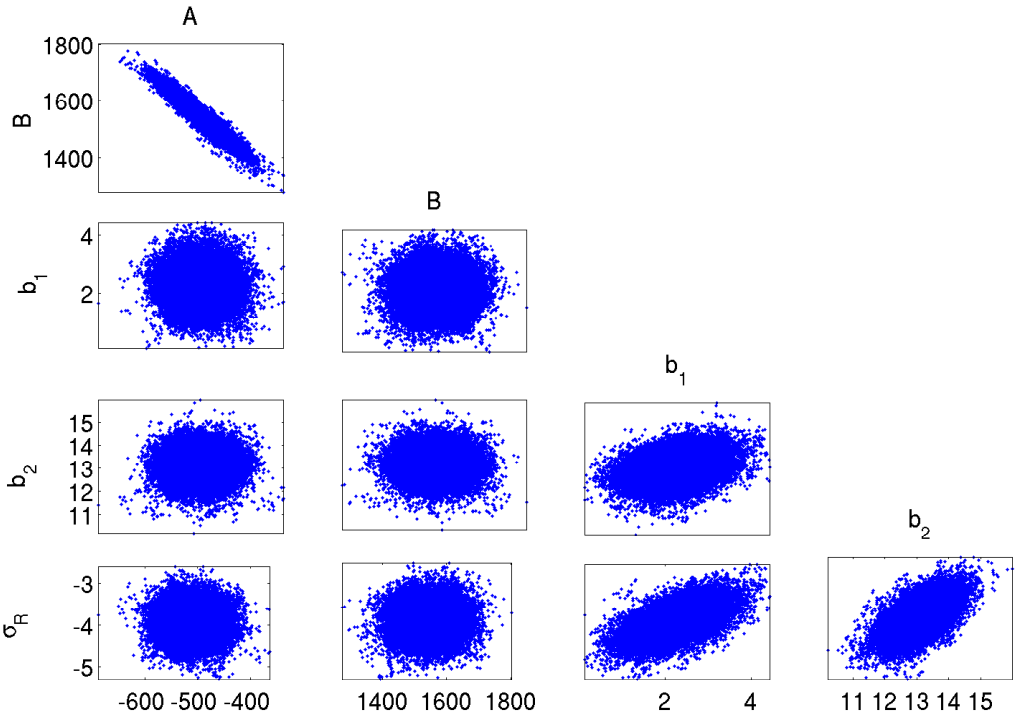

Figure 7. Correlation between all five parameters illustrating strong correlation only between the A and B Landau parameters.

Robust energy functions will require a broader range of atomic configurations and

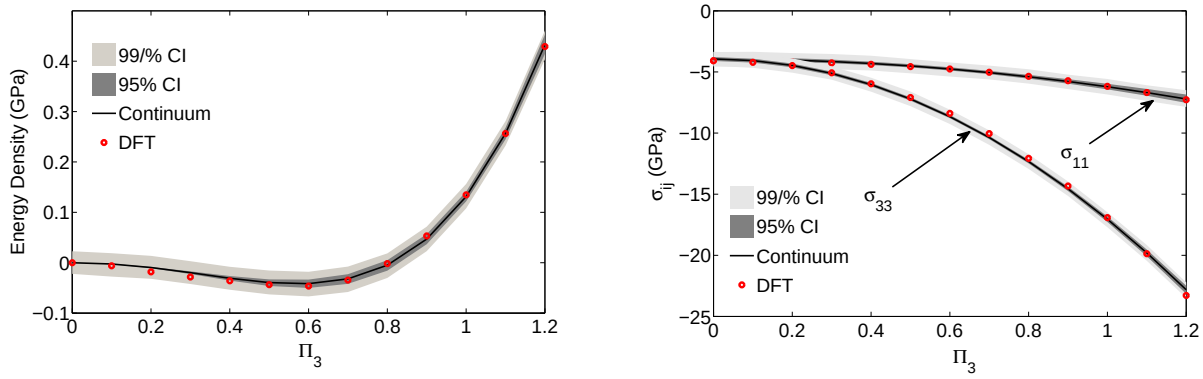

(a) (b)

Figure 8. Uncertainty propagation illustrating 99% and 95% confidence intervals based upon the Bayesian uncertainty quantification. The mean continuum estimates are given by the black lines and the DFT solutions are given at each discrete point.

corresponding electronic states as well as different deformation states. Simulation of shear deformation may result in higher material parameter uncertainty associated with the shear electromechanical coupling parameter b_3 and Landau parameter C. Larger supercells may be necessary to accurately calculate anti-symmetric shear deformation since most DFT codes are based on periodic electronic structure calculations. Bayesian statistics are expected to serve as a useful tool to guide the number of vector order parameters (i.e, $\nu \geq 1$) and its functional form within the stored energy. This is expected to be crucial for development of quantum-based homogenized ferroelectric models that can handle more complicated electromechanical loads and integration into microstructure phase field methods that simulate domain structure evolution.

Acknowledgments

The author appreciates useful discussion with Kaushik Bhattacharya regarding the DFT calculations. The author also appreciates many useful discussions with Ralph Smith about Bayesian statistics. This material is based upon work supported by an NSF CDS&E award (grant 1306320). Any opinions, findings, and conclusions or recommendations expressed in this publication are those of the author and do not necessarily reflect the views of the funding sponsor.

References

Bilc D I, Orlando R, Shaltaf R, Rignanese G M, Íñiguez J & Ghosez P 2008 *Phys. Rev. B* **77**, 165107. **URL:** *http://link.aps.org/doi/10.1103/PhysRevB.77.165107*

Catalan G, Lubk A, Vlooswijk A H G, Snoeck E, Magen C, Janssens A, Rispens G, Rijnders G, Blank D H A & Noheda B 2011 *Nat. Mat.* **10**, 963–967.

Cross E 2006 *J. Mat. Sci.* **41**, 53–63.

Eom C & Trolier-McKinstry S 2012 *MRS Bulletin* **37**, 1007–1017.

Feynman R 1939 *Phys. Rev.* **56**, 340–343.

Finnis M 2012 *MRS Bulletin* **37**, 477–484.

Gonze X, Amadon B, Anglade P M, Beuken J M, Bottin F, Boulanger P, Bruneval F, Caliste D, Caracas R, Cote M, Deutsch T, Genovese L, Ghosez P, Giantomassi M, Goedecker S, Hamann D, Hermet P, Jollet F, Jomard G, Leroux S, Mancini M, Mazevet S, Oliveira M, Onida G, Pouillon Y, Rangel T, Rignanese G M, Sangalli D, Shaltaf R, Torrent M, Verstraete M, Zerah G & Zwanziger J 2009 *Computer Physics Communications* **180**(12), 2582–2615.

Haario H, Laine M, Mira A & Saksman E 2006 *Statistics and Computing* **16**(4), 339–354.

Haario H, Saksman E & Tamminen J 2001 *Bernoulli* **7**(2), 223–242.

Hu Z, Smith R, Burch N, Hays M & Oates W 2012 *J. Intell. Mater. Sys. Struct. (accepted)* .

Jaffe B, Cook W & Jaffe H 1971 *Piezoelectric Ceramics* Academic Press London.

Lee D, Yoon A, Jang S Y, Yoon J G, Chung J S, Kim M, Scott J F & Noh T W 2011 *Phys. Rev. Lett.* **107**, 057602. **URL:** *http://link.aps.org/doi/10.1103/PhysRevLett.107.057602*

Lines M & Glass A 1977 *Principles and Applications of Ferroelectrics and Related Materials* Clarendon Press Oxford.

Loudon R 2000 *The Quantum Theory of Light* Oxford University Press Oxford.

Lynch C 1996 *Acta. Mater.* **44**(10), 4137–4148.

Mabud S A & Glazer A M 1979 *Journal of Applied Crystallography* **12**(1), 49–53.
URL: *http://dx.doi.org/10.1107/S0021889879011754*

Malvern L 1969 *Introduction to the Mechanics of a Continuous Medium* Prentice-Hall, Inc. Englewood Cliffs, NJ.

Martin R 1972 *Phys. Rev. B* **5**(4), 1607–1613.

Nelson D 1979 *Electric, Optic, and Acoustic Interactions in Dielectrics* John Wiley and Sons New York.

Nelson D 1991 *Phys. Rev. A* **44**(6), 3985–3996.

Panofsky W & Phillips M 1962 *Classical Electricity and Magnetism* Addison-Wesley Publishing Company, Inc. Reading, MA.

Payne M C, Teter M P, Allan D C, Arias T A & Joannopoulos J D 1992 *Rev. Mod. Phys.* **64**, 1045–1097.
URL: *http://link.aps.org/doi/10.1103/RevModPhys.64.1045*

Resta R 2010 *Phys. Rev. Lett.* **105**, 127601.

Resta R & Vanderbilt D 2007 *in* 'Physics of Ferroelectrics' Vol. 105 of *Topics in Applied Physics* Springer Berlin Heidelberg pp. 31–68.

Shirane G, Pepinsky R & Frazer B C 1956 *Acta Crystallographica* **9**(2), 131–140.
URL: *http://dx.doi.org/10.1107/S0365110X56000309*

Smith R 2005 *Smart Material Systems: Model Development* SIAM Philadelphia, PA.

Weiner J H 1983 *Statistical Mechanics of Elasticity* John Wiley & Sons New York.

Yang S, Seidel J, Byrnes S, Shafer P, Yang C, Rossell M, Yu P, Chu Y H, Scott J, Ager J, Martin L & Ramesh R 2010 *Nature Nanotechnology* **5**, 143–147.